Geomechanical Deformation of Saturated Porous Media under Various Wettability Conditions: A Pore-scale Investigation

Ahmed Zankoor[1, *], *Rui* Wang[1], *Maziar* Arshadi[1], and *Mohammad* Piri[1]

[1] Center of Innovation for Flow through Porous Media, Department of Petroleum Engineering, University of Wyoming, Laramie, WY, USA.

Abstract. Geomechanical deformation may occur during various engineering processes that involve fluid flow in the subsurface, such as hydrocarbon recovery, groundwater withdrawal, and CO_2 sequestration. However, its impact on multiphase flow in porous media is still poorly understood due to the limited research on this topic at the pore scale level. In this study, we investigate the effects of pore space deformation on pore-scale fluid occupancies and in-situ capillary pressures of two companion miniature sand packs under different wettability conditions. To this end, the samples were first subjected to drainage (oil-dispalcing-water) processes, one using Soltrol and other with dead crude oil, to establish different wettability states in the samples. The mediums were then contracted by increasing the hydrostatic (radial and axial) stresses. The fluid occupancies and the fluid-fluid interfacial curvatures under different stress conditions were acquired using high-resolution x-ray computed tomography and advanced image analysis techniques. The results of our investigations showed that as the pore space contracted due to the hydrostaic stress, a decrease in the oil saturation was observed in both samples but to a lesser extent and less uniformity in the oil-wet case. Similarly, the in-situ capillary pressure measurements showed a more uniform and significant reduction after the compression in the water-wet sample. Nonetheless, local increases in the in-situ capillary pressure were observed in the oil-wet sample. Capillary pressure reductions or increases were attributed to interfaces being displaced or hinged in place in response to the compression process.

1. Introduction

Fluid extraction or injection from/into subsurface reservoirs causes variations in the effective stresses which in turn may cause geomechanical deformation. The deformation of porous media has critical impacts on the multiphase flow phenomena at micro- and macro-scale levels and, under certain circumstances, may result in field-scale implications such as land subsidence and induced fractures and fissures [1, 2].

Over the decades, one of the most common methods used to investigate the impacts of the pore space deformation on multiphase flow and fluid distribution in porous media was measuring the saturation-relative permeability data under various stress conditions. However, inconsistent or even contradictory results have been reported in the literature. By increasing the hydrostatic confining pressure and maintaining the pore pressure constant, multiple researchers reported that the relative permeability of the non-wetting phase decreased significantly, whereas that of the wetting phase was nearly remained unchanged [3, 4, 5]. By contrast, a different trend was also reported in the literature [6, 7, 8]. In these studies, the relative permeabilities of the wetting and non-wetting phases were found to decrease and increase, respectively, as the confining pressure was increased. In addition to these two dominant viewpoints, some other conclusions have been reached, such as that neither the wetting nor the non-wetting phase relative permeabilities were sensitive to the changes in the stress [9, 10].

The lack of consensus on the impacts of geomechanical deformation on fluid flow is partly due to the limited understanding of the pore-scale mechanisms accompanying this phenomenon, because the previous – predominantly Darcy scale – experiments do not provide insight into underlying pore-scale physics that govern the macroscopic behavior of such systems.

The recent advances in x-ray microtomography imaging have provided a new window of opportunity to directly observe the multi-phase flow phenomena in such systems and further advance the understanding of the flow behavior on the pore-scale level. However, the application of these technologies to investigate geomechanical deformation is still at its early development stages and pore-scale studies in such area are scarce at best. The impacts of the pore space deformation on the fluid occupancy were studied by Torrealba et al. (2016) [11]. They observed that primary drainage established different initial water saturation profiles along a glass bead pack under various stress conditions even though the average saturations were similar. Moreover, they reported that the residual oil saturation decreased when waterflooding was performed simultaneously with the sample's compression, whereas it was negligibly affected if the sample was compressed after the residual oil was trapped.

* Corresponding author: azankoor@uwyo.edu

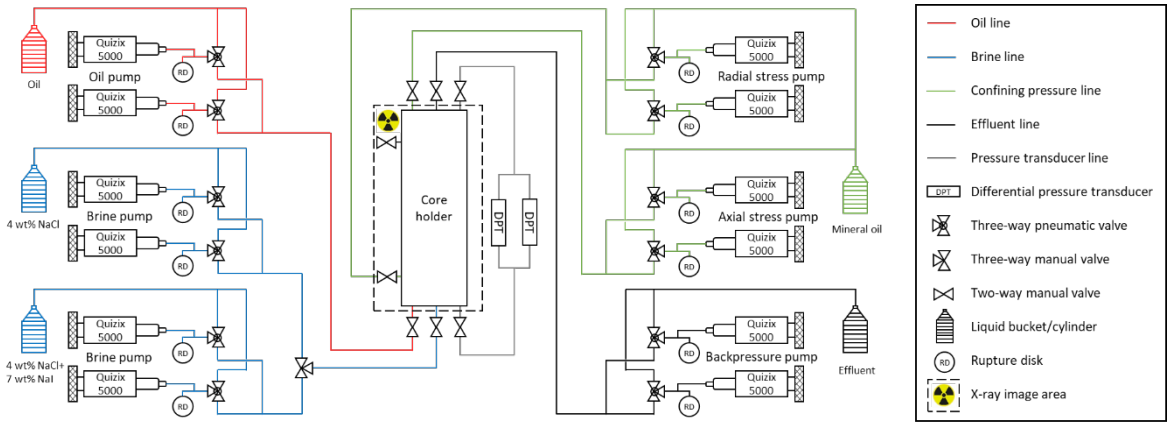

Fig.1. Schematic diagram of the experimental setup used in this study.

In the current research, we provide, to our best knowledge, the first pore-scale investigations of the impact of wettability on the response of the fluids in porous media to geomechanical deformation. We provide an improved understanding of such processes by extending our previous investigations [12, 13] to probe the interrelationship between pore-scale capillary pressure and fluid occupancy when pore space is compacted.

2. Experiments and data acquisition

The experimental data used in this study was generated by Wang et al. [12, 13] during a set of micro-scale core flooding experiments. In this section, we provide brief descriptions of the rock sample and fluids as well as the experimental apparatus and procedure used to obtain the data. More details can be found in the original work.

2.1. Sample and fluids

Two miniature sandpack samples, each with a diameter of 10 mm and a length of 75 mm, were used as the samples in the water- and oil-wet experiments to observe remarkable pore space deformation at lower stress conditions. Such deformation was necessary to observe significant impacts on the pore-scale fluid configuration and flow properties compared to less significant responses of other porous media (e.g., consolidated rocks). Moreover, the sandpack sample could represent unconsolidated reservoirs, which are expected to deform prominently as stress varies. The sandpack grains were the high-roundness and high-sphericity Northern White monocrystalline sands (100 weight % SiO_2) with the diameters varying from 106 to 300 microns (100 mesh). To ensure the two samples had similar properties, the two sandpacks were prepared using an identical preparation technique, which was developed based on the method proposed by the University of Alberta [14, 15, 16]. Instead of raining the sands into liquid, we densified the dry sands by vibrating for 2 hours to eliminate any bedding or sedimentary sequence caused by the different setlling rates of large and small grains during the deposition process [17]. This is because the resistance of air is negligible compared to liquid, and grains with different sizes and shapes are more likely to deposit with the similar speed in air [18]. Afterward, the sands were partially filled by distilled water through spontaneous imbibition and frozen in liquid nitrogen. This allowed for preventing the samples from collapsing and maintaining their properties unchanged when they were transported to the core holder.

The aqueous phase used in the water- and oil-wet experiments was a 4 wt% NaCl + 7 wt% NaI brine solution. The purpose of adding NaI was to increase the x-ray attenuation in the brine and obtain a better contrast between the brine and oil in the two-phase fluid occupancy images. The oil phases used in the water- and oil-wet experiments were Soltrol 170 mineral oil and dead crude oil recovered from the Permian Basin in Texas, respectively. The Soltrol 170 was passed through layers of silica gel and alumina multiple times before the main tests to remove all the polar components that might alter the wettability of the sandpack sample. All the solid particles that were larger than 5 micrometer were filtered from the crude oil in advance to avoid blocking the pore space during the flow tests. The properties of the sandpack and fluids used in this study are listed in Tables 1 and 2.

Table 1. Porosities and permeabilities of the two sandpack samples used in the water- and oil-wet experiments at the effective stress of 100 psi.

Sample	Porosity	Permeability (D)
A (water-wet)	0.302	6.59
B (oil-wet)	0.306	7.58

Table 2. Properties of the fluids used in this study at ambient temperature and pressure.

Fluid	Density (g/cc)	Viscosity (cp)	Oil/Brine IFT (mN/m)
Brine	1.07	1.06	
Sotrol 170	0.78	2.92	41.3
Crude oil	0.83	5.60	14.9

2.2. Experimental setup and procedure

The experimental setup used for the water- and oil-wet experiments is comprised of the following components: a high-resolution x-ray micro-CT scanner used to scan the sample and acquire the fluid occupancy during the experiment and a high-pressure and high-temperature core-flooding system, which consisted of an X-ray transparent miniature core holder made of carbon fiber, multiple Quizix pumps, two differential pressure transducers, and tubing. The schematic of the apparatus is shown in **Fig.1**.

Before starting the experiments, the sandpack sample was left in the core holder at an effective stress of 100 psi for three hours until it was completely thawed. It was then dried by blowing CO_2 at 30 psig for another three hours and vacuumed overnight. After the sample was 100% saturated by the doped brine (4 wt% NaCl + 7wt% NaI) both the pore pressure and the hydrostatic confining pressure were gradually increased to the target values by the backpressure regulation pump and the confining pumps (the radial and axial stress pumps). The initial permeability was measured by performing a series of brine flow tests at various flow rates and recording the pressure drops using the differential pressure transducers. To obtain the pore network before the compression, a high-resolution scan was performed after the doped brine was displaced by the one without the NaI. Then the pore space was filled by the doped brine again before the oil phase was introduced into the pore space. Note that the doped brine must be used to saturate the sample and fill the dead volumes after the system was vacuumed. It aimed to avoid diffusion caused by the concentration difference of iodine ions between the dead volumes and the sandpack sample. Otherwise, oil/water interfaces may become blurry during the experiment.

During the main experiments, oil was initially injected into the sandpack sample at 0.01 cc/min. The oil flow rate was then gradually increased until a target initial water saturation (Swi= 20 to 30%) was confirmed by the fluid occupancy images acquired by micro-CT scans. At this stage, we stopped the oil injection and increased the hydrostatic confining pressures to the pre-determined value in 8 hours, which was expected to be longer than the normal relaxation time after a change in phase saturation in a unconsolidated porous medium [19], in the water-wet experiment. Stopping the oil injection aimed to eliminate the impacts of fluid flow on fluid occupancy. In other words, any fluid redistribution observed in the new fluid occupancy acquired after the compression could be ascribed to the pore space contraction.

In the oil-wet experiment, dynamic aging was performed before stopping the flow and increasing the confining pressure to alter the wettability of the sandpack sample. We heated the sample at 50 °C and simultaneously injected the dead crude oil at a low flow rate of 0.002 cc/min. This allowed for making up for the loss of the polar components that reacted with the solid surfaces. During the dynamic aging, we injected 0.1 to 0.5 pore volume of brine every 7 to 10 days (partial waterflooding) to mobilize the oil-water interfaces and measured the in-situ contact angles on the fluid occupancy images. After each measurement, the initial fluid occupancy was restored by oil injection. **Fig. 3** shows oil-water interfaces in both the water- and oil-wet cases during the partial waterflooding processes. Overall, the average in-situ contact angle at the end of primary drainage was 41.7° in the water-wet case while in the oil-wet case it increased with time during the dynamic aging process and stabilized at 107° after 5 weeks. More details about the in-situ wettability mesaurements can be found elsewhere [12, 13].

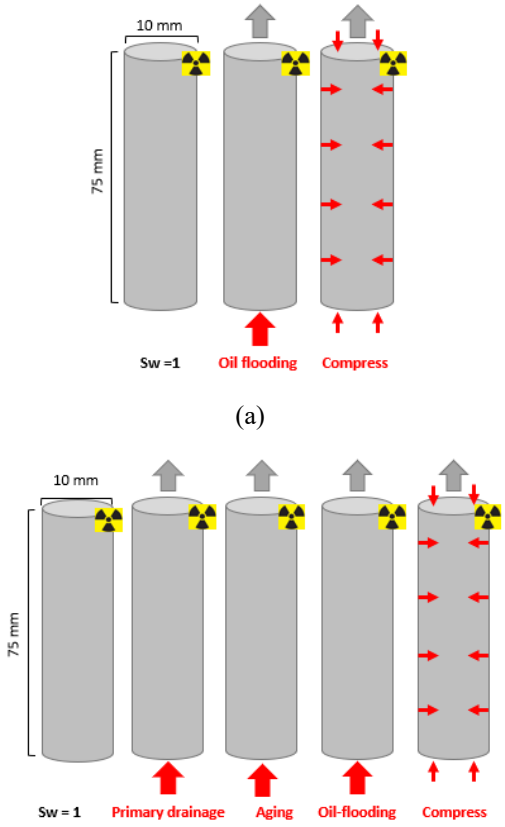

Fig. 2. Schematic diagrams of the experimental procedures followed in the (a) water-wet and (b) oil-wet experiments (replotted after Wang et al. (2022) *[12, 13]*).

3. Image analysis

The raw grayscale images acquired during the core-flooding experiments were processed using Avizo software [20]. They were first filtered using 3D non-local means and median filters to improve the signal-to-noise ratio, registered and superimposed by the corresponding pore map (before or after the compression), and subsequently segmented using the interactive thresholding method to generate the pore-scale fluid occupancy maps, i.e., images with unique labels assigned to the oil, aqueous, and solid phases. The fluid occupancy maps were then used to quantify the fluid volume/saturation along the flow direction. We also characterized the in-situ capillary pressure using the interfacial curvature analysis method described by Zankoor et al. [21]. In this method, the pore-scale oil-water interfaces were first extracted from the segmented images and then

smoothened to reduce the impact of voxelization on curvature analysis. Subsequently, the local curvature values were computed at each point of the interface, and the average of all curvature values was found to calculate the local capillary pressure using the Young-Laplace equation:

$$P_{c_{ow}} = P_o - P_w = \sigma_{ow} K_T \quad (1)$$

where $P_{c_{ow}}$ is the oil-water capillary pressure in Pa, P_o and P_w are the oil and water pressures, respectively, in Pa, σ_{ow} denotes the interfacial tension between the oil and water phases in N/m, and K_T is the average total curvature of the interface in m^{-1} (i.e., summation of the principal curvatures).

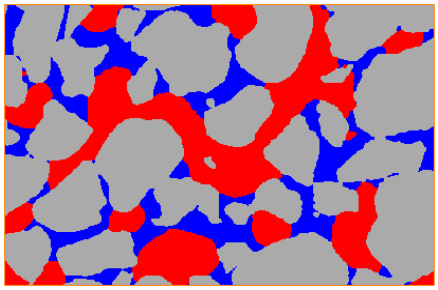

(a)

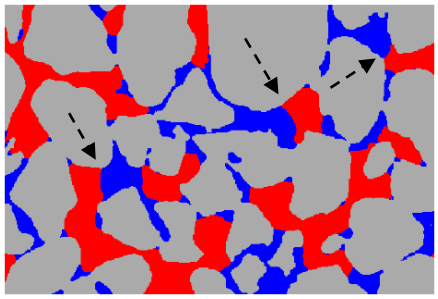

(b)

Fig. 3. Pore-scale fluid occupancy during partial waterflooding processes on the (a) **water-wet** and (b) **oil-wet** samples. Oil-water interfaces bulging in the oil-phase (black arrows in (b)) confirm the establishment of the oil-wet conditions.

4. Results and discussion

As explained in the materials & method section, the two sandpack samples were subjected to oil flooding and then compression processes. The first sample was flooded with filtered Soltrol to maintain a water-wet medium. The second sample was desaturated with and dynamically aged using the dead crude oil to alter the wettability of the medium to non-water-wet states. The initial water saturations (S_{wi}) established after these processes were found to be 0.31 and 0.2, respectively. The lower S_{wi} in the oil-wet case was attributed to the lower interfacial tension and higher viscosity of the crude oil which improved the water displacement efficiency (see **Fig. 4**(a) and **Fig. 5**(a)). The subsequent compression processes squeezed the samples causing contraction of the pore space and the close-up of some pore elements, as illustrated by the dashed circles in **Fig. 4**(b) and **Fig. 5**(b), and, in turn, expelled fluid(s) out of the samples. **Fig. 6**(a) and **Fig. 7**(a) show the oil volume profiles along the flow direction before and after compression for the water- and oil-wet samples, respectively. In the water-wet sample, the oil volume reduced significantly and uniformly across the medium. In addition to pore space contraction, this reduction was found to be partly induced by water flow from outside the field of view (FOV) displacing oil from the FOV. This imbibition-like process caused considerable water-to-oil displacements. Therefore, interfaces were pushed toward wider regions in the pore space, as indicated by the black arrows in **Fig. 4**(b). These displacements were associated with significant reductions in the interfacial curvatures and the respective capillary pressure values as shown in **Fig. 6** (b).

In the oil-wet sample, the response to the compression process was relatively more heterogeneous across the sample compared to the water-wet case. As displayed in **Fig. 7**(a), the oil volume reduction was less compared to that in the water-wet case. In particular, the volume and relative volume changes (ΔVo and $(\Delta Vo/Vo) \times 100$) in the oil-wet sample were -1.26E+06 μm^3 and -6 % compared to -2.96E+06 μm^3 and -18% in the water-wet case. This is attributed to the lower affinity of the porous medium to expel the oil phase in the oil-wet sample. It is also observed that in the oil-wet sample, the oil volume reduction at the two ends of the FOV is more significant compared to the middle which requires further investigations.

The in-situ capillary pressure profile along the z-axis of the oil-wet sample (flow direction within FOV) is shown in **Fig. 7**(b). First, it can be noted that the capillary pressure values in the oil-wet sample are smaller than those in the water-wet case (by around one order of magnitude). This is consistent with the oil-wet condition established after the dynamic aging process since more interfaces are expected to have negative curvatures. The profile revealed that the compaction of the oil-wet sample caused the local capillary pressure to change nonuniformly across the medium. The local capillary pressure slightly decreased or remained unchanged at the two ends, while it increased at the middle part. The behavior at the two ends can be attributed to the significant reduction in the oil volume at these locations (as shown in **Fig. 7**(a)), which implies that oil was displaced, and interfaces moved toward wider regions in the pore space. On the other hand, the behavior in the middle part of the sample may imply less significant displacement of the interfaces accompanying the compression process. As a result, the pore space contraction may cause the interfaces to hinge in place and become more curved. In **Fig. 5**(b), yellow point to locations where oil-water interfaces experienced insignificant displacements and hinged in-place in response to the compression process. In other words, interfaces may bear part of the stress caused by the compression process. These hypotheses will be further investigated in future studies.

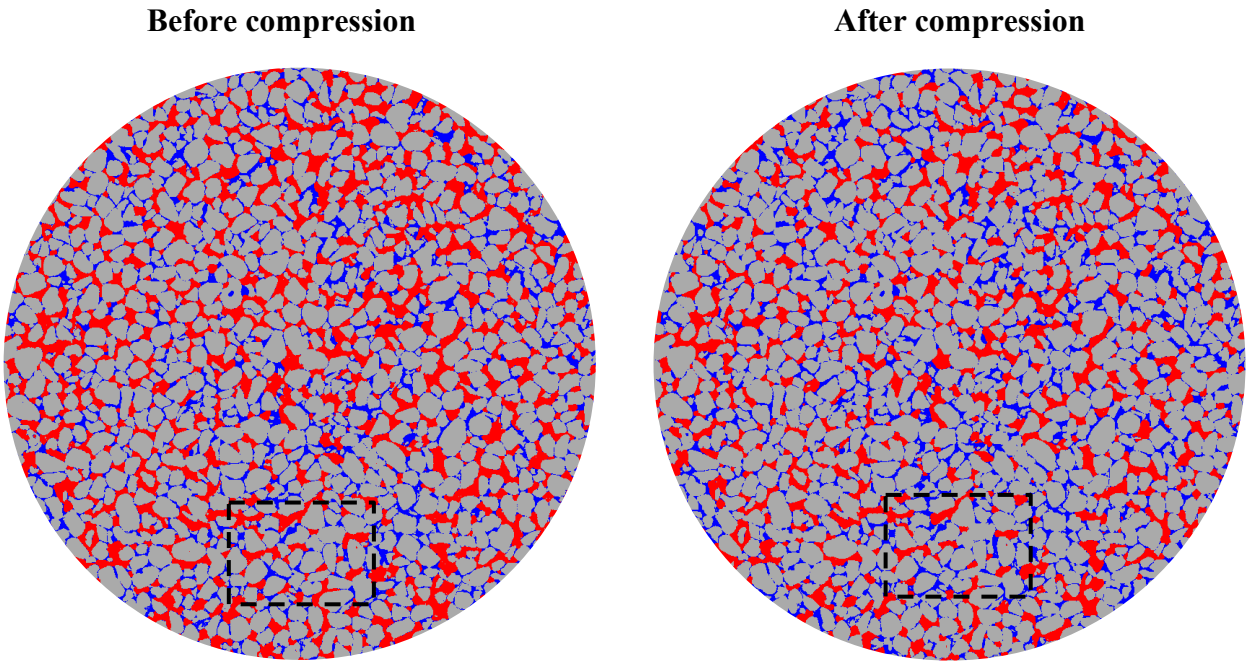

(a) Pore-scale fluid occupancy maps of the entire FOV with oil, brine and grains shown in red, blue and grey, respectively.

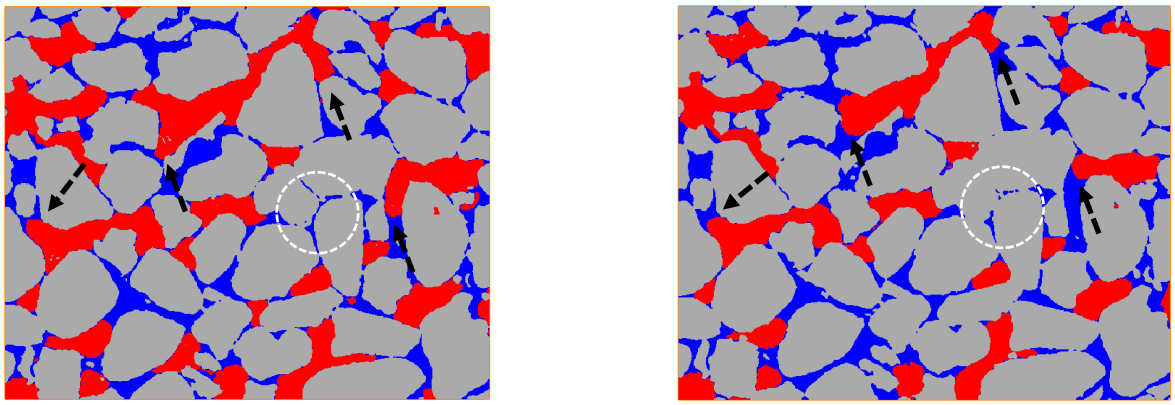

(b) Magnified view of the dashed areas in (a). The black arrows point to oil-water interfaces displaced through water-to-oil displaced through water-to-oil displacements in response to the compression process.

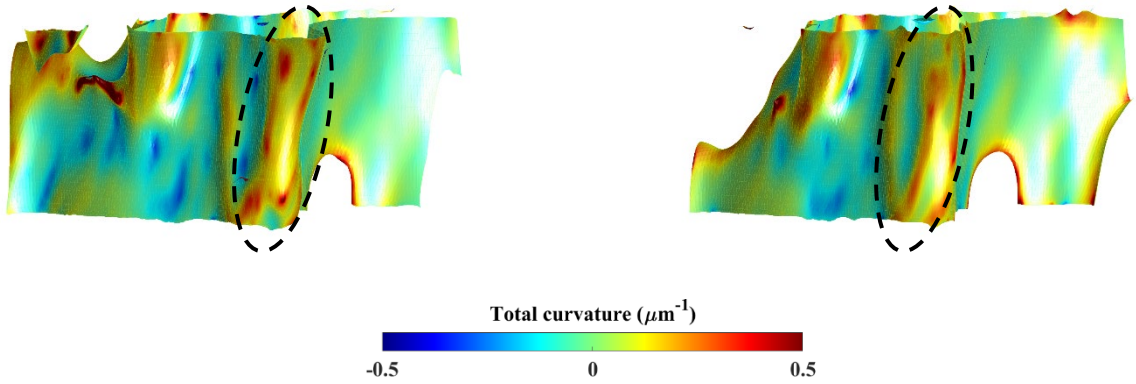

(c) Example of oil interfaces color-coded based on the curvature values. The dashed areas show reduction in the interfacial curvature due to the compression process.

Fig. 4. Two and three dimentional visualizations of the **water-wet** sample before (left column) and after (right column) compression.

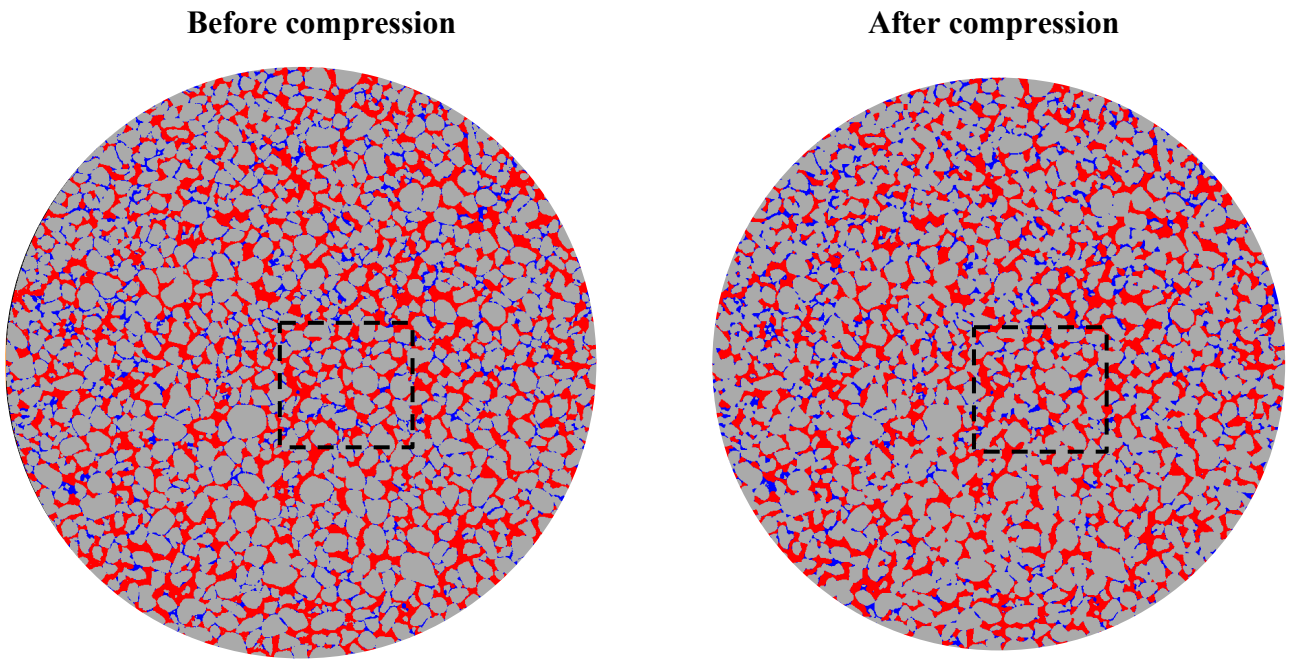

(a) Pore-scale fluid occupancy maps of the entire FOV with oil, brine and grains shown in red, blue and grey, respectively.

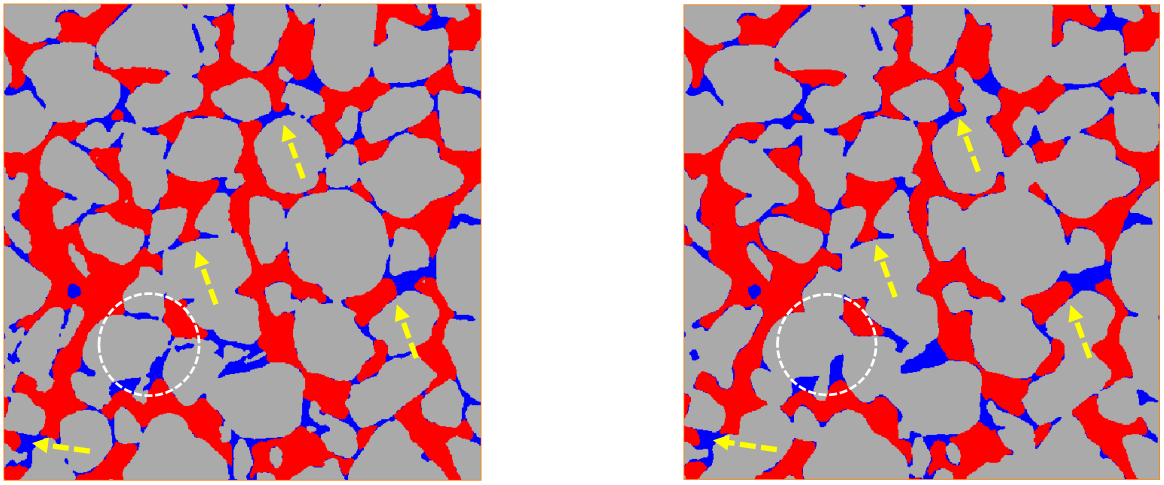

(b) Magnified view of the dashed areas in (a). The yellow arrows point to oil-water interfaces hinging in place in response to the compression process.

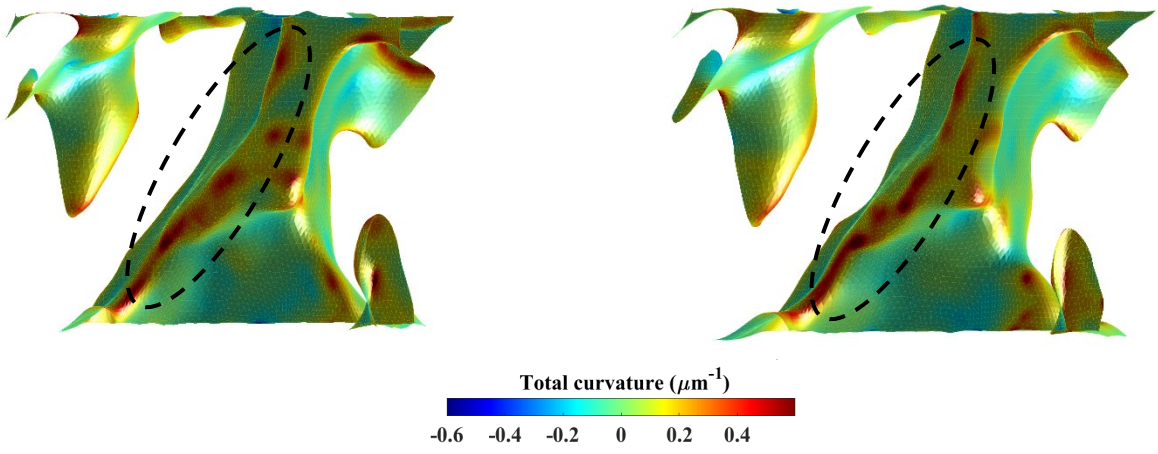

(c) Example of oil interfaces color-coded based on the curvature values. The dashed areas show increases in the interfacial curvature due to the compression process.

Fig. 5. Two and three dimentional visualizations of the **oil-wet** sample before (left column) and after (right column) compression.

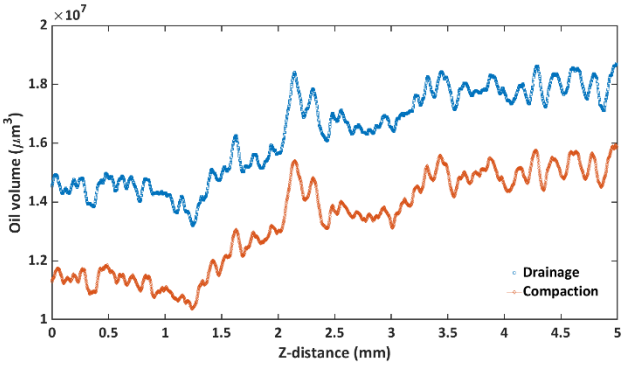

(a)

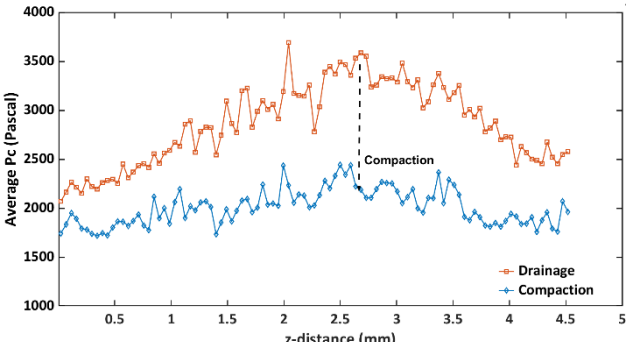

(b)

Fig. 6. Oil volume (a) and in-situ capillary pressure (b) profiles along the flow direction of the water-wet sample during oil flooding and compaction processes.

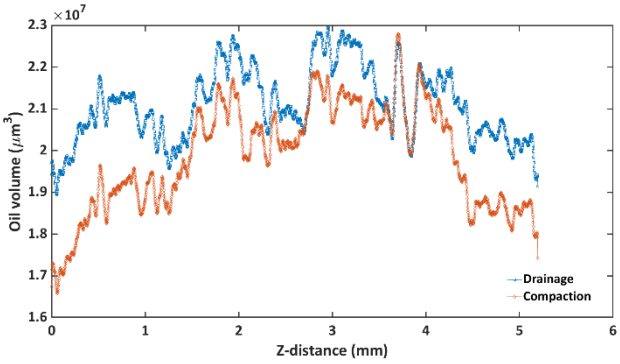

(a)

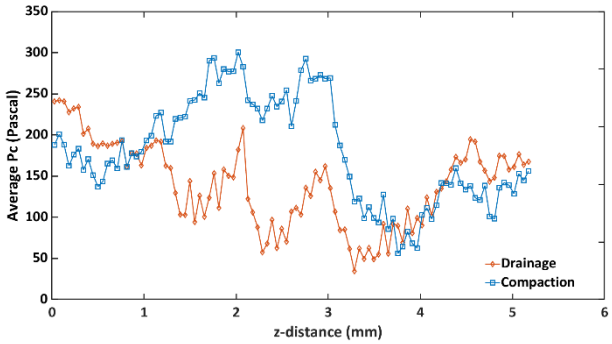

(b)

Fig. 7. Oil volume (a) and in-situ capillary pressure (b) profiles along the flow direction of the oil-wet sample during oil flooding and compaction processes.

4. Conclusions

Pore-scale images of water- and oil-wet miniature sandpack samples were acquired under low and high stress conditions. The two samples were subjected to oil drainage processes and then compressed hydrostatically to similar stress levels. The acquired images were analyzed to obtain fluid volume and in-situ capillary pressure profiles across the imaging FOV. The results of this study showed that the pore space contraction caused reduction in the oil volume in both samples indicating oil desaturation. However, unlike the water-wet sample, this reduction was less uniform in the oil-wet sample with less significant changes in the middle region of the FOV. The in-situ capillary pressure measurements also showed a general reduction trend which is attributed to displacement of interfaces to wider regions in the pore space due to the contraction. Nevertheless, local increases in capillary pressure were observed in the middle part of the oil-wet sample which was associated with pinned interfaces hinging in place and experiencing increase in their curvature accompanying the pore-space contraction.

We gratefully acknowledge the financial support of Thermo Fisher Scientific, Hess Corporation, and the University of Wyoming. We also thank the reviewers Dr. Steffen Berg and Dr. Will Richardson for their detailed revision and constructive comments.

References

[1] G. Gambolati and P. Teatini, "Geomechanics of subsurface water withdrawal and injection," *Water Resources Research,* vol. 51, 2015.

[2] G. Alexander E. and C. George V., "Subsidence over producing oil and gas fields, and gas leakage to the surface," *Journal of Petroleum Science and Engineering,* vol. 9, 1993.

[3] H. S. Ali, M. A. Al-Marhoun, S. A. Abu-Khamsin and M. S. Celik, "The Effect of Overburden Pressure on Relative Permeability," *Middle East Oil Show, Bahrain,* 1987.

[4] C. Jones, A. Al-Quraishi, J. Somerville and S. A. Hamilton, "Stress sensitivity of saturation and end-point relative permeabilities," *Society of core analysts, Edinburgh, Scotland,* 2001.

[5] A. Gawish and E. Al-Homadhi, "Relative permeability curves for high pressure, high temperature reservoir conditions," *Oil Gas Bus,* vol. 2, 2008.

[6] D. Chen, Z. Pan, J. Liu and L. D. Connell, "An improved relative permeability model for coal reservoirs," *International Journal of Coal Geology,* 2013.

[7] M. K. Dabbous, A. A. Reznik, J. J. Taber and P. F. Fulton, "The Permeability of Coal to Gas and Water," *Society of Petroleum Engineers Journal,* vol. 14.

[8] J. W. Wilson, "Determination of relative permeability under simulated reservoir," *AIChE Journal,* vol. 2, 1956.

[9] I. Fatt, "The Effect of Overburden Pressure on Relative Permeability," *Journal of Petroleum Technology,* vol. 5, 1953.

[10] R. D. Thomas and D. C. Ward, "Effect of Overburden Pressure and Water Saturation on Gas Permeability of Tight Sandstone Cores," *Journal of Petroleum Technology,* vol. 24, 1972.

[11] V. A. Torrealba, Z. T. Karpyn, H. Yoon, K. A. Klise and D. Crandall, "Pore-scale investigation on stress-dependent characteristics of granular packs and the impact of pore deformation on fluid distribution," *Geofluids,* vol. 16, 2016.

[12] R. Wang, M. Arshadi, A. Zankoor and M. Piri, "Pore space deformation and its implications for two phase flow through porous media: A micro scale experimental investigation," *(Submitted),* 2022.

[13] R. Wang, M. Arshadi and M. Piri, Impacts of pore space deformation on two-phase flow in unconsolidated porous media under various wettability conditions, In preparation, 2022.

[14] M. Hamoud, "Influence of geomechanical processes on relative permeability," *(Mater's thesis). Retrieved from [ProQuest]. Edmonton, Alberta: University of Alberta.,* 2012.

[15] M. Pazouki, "An experimental study on oil sand lump ablation," *(Doctoral dissertation). Retrieved from [ProQuest]. Edmonton, Alberta: University of Alberta.,* 2013.

[16] X. Wang, R. Chalaturnyk, H. Huang and J. Leung, "Permeability Variations Associated with Various Stress State during Pore Pressure Injection.," *Paper presented at 49th U.S. Rock Mechanics/Geomechanics*

Symposium, San Francisco, California., 2015.

[17] R. Ferguson and M. Church, "A Simple Universal Equation for Grain Settling Velocity," *Journal of Sedimentary Research,* vol. 74, no. 6, p. 933–937, 2004.

[18] E. Farrell and D. Sherman, "A new relationship between grain size and fall (settling) velocity in air. ," *Progress in Physical Geography: Earth and Environment.,* vol. 39, no. 3, pp. 361-387, 2015.

[19] S. Schlüter, S. Berg, T. Li, H.-J. Vogel and D. Wildenschild, "Time scales of relaxation dynamics during transient conditions in two-phase flow," *Water Resources Research,* vol. 53, no. 6, pp. 4709-4724, 2017.

[20] M. Khishvand, A. Alizadeh and M. Piri, "In-situ characterization of wettability and pore-scale displacements during two- and three-phase flow in natural porous media," *Adv. in Water Res.,* 2016.

[21] A. Zankoor, M. Khishvand, A. Mohamed, R. Wang and M. Piri, "In-situ capillary pressure and wettability in natural porous media: Multi-scale experimentation and automated characterization using x-ray images," *Journal of Colloid and Interface Science,* 2021.